Lawrence Berkeley National Laboratory

Title
Global terrestrial stilling: does Earth's greening play a role?

Permalink
https://escholarship.org/uc/item/4s81s8v6

Journal
Environmental Research Letters, 13(12)

ISSN
1748-9318

Authors
Zeng, Zhenzhong
Piao, Shilong
Li, Laurent ZX
et al.

Publication Date
2018

DOI
10.1088/1748-9326/aaea84

Global terrestrial stilling: does Earth's greening play a role?

To cite this article: Zhenzhong Zeng *et al* 2018 *Environ. Res. Lett.* **13** 124013

View the article online for updates and enhancements.

Environmental Research Letters

LETTER

CrossMark

Global terrestrial stilling: does Earth's greening play a role?

Zhenzhong Zeng[1,2] ⓘ, Shilong Piao[1,3] ⓘ, Laurent Z X Li[4], Philippe Ciais[5], Yue Li[1], Xitian Cai[6], Long Yang[2], Maofeng Liu[2] ⓘ and Eric F Wood[2]

1   Sino-French Institute for Earth System Science, College of Urban and Environmental Sciences, Peking University, Beijing 100871, People's Republic of China
2   Department of Civil and Environmental Engineering, Princeton University, Princeton, NJ 08540, United States of America
3   Institute of Tibetan Plateau Research, Chinese Academy of Sciences, Beijing 100085, People's Republic of China
4   Laboratoire de Météorologie Dynamique, Centre National de la Recherche Scientifique, Université Pierre et Marie Curie-Paris 6, F-75252 Paris, France
5   Laboratoire des Sciences du Climat et de l'Environnement, UMR 1572 CEA-CNRSUVSQ, F-91191 Gif-sur-Yvette, France
6   Climate and Ecosystem Sciences Division, Lawrence Berkeley National Laboratory, Berkeley, CA 94720, United States of America

E-mail: slpiao@pku.edu.cn

Abstract

Previous studies have documented that surface wind speed (u) has been increasing over the ocean but decreasing over land for the past several decades. The decreasing u at the surface over land has been referred to as terrestrial stilling. A plausible hypothesis for terrestrial stilling is an increase in surface roughness associated with changes in land surface (e.g. enhanced vegetation growth, landscape fragmentation or urbanization). One of the most widespread land surface changes is enhanced vegetation leaf area index (LAI) known as greening, particularly over the middle to high latitudes of the Northern Hemisphere where strong stilling is observed from weather station data. In this study, we examine the hypothesis that enhanced vegetation LAI is a key driver of global terrestrial stilling. We first characterized the trend in u over the ocean using long-term satellite altimeter measurements, and the trend in u over land using continuous wind records from 4305 *in situ* meteorological stations. We then performed initial condition ensemble Atmospheric Model Intercomparison Project-type simulations using two state-of-the-art Earth system models (IPSL-CM and CESM) to isolate the response of u to the historical increase in LAI (representing the greening) for the period 1982–2011. Both models, forced with observed sea surface temperature and sea ice and with LAI from satellite observation, captured the observed strengthening of Pacific trade winds and Southern Ocean westerly winds. However, these simulations did not reproduce the weakening of surface winds over land as significantly as it appears in the observations (-0.006 m s^{-1} versus -0.198 m s^{-1} during 1982–2011), indicating that enhanced LAI (greening) is not a dominant driver for terrestrial stilling.

1. Introduction

Surface wind speed (u) is the kinetic energy of the atmosphere that influences turbulent fluxes of water, energy, and momentum between the atmosphere and land or ocean surfaces. A change in u is an important manifestation of climate change, in addition to temperature and precipitation trends. While u over oceans has been increasing during the past 30 years (Wentz *et al* 2007, Young *et al* 2011, Zheng *et al* 2016), u measured at *in situ* weather stations at 10 m above

ground has significantly decreased over land, particularly in the middle to high latitudes of the Northern Hemisphere (Vautard *et al* 2010, McVicar *et al* 2012b, Wu *et al* 2018). This phenomenon has been referred to as terrestrial stilling (Roderick *et al* 2007), and it has important scientific, socioeconomic, and environmental implications for fields including, but not limited to, agriculture and hydrology (McVicar *et al* 2012a), wind energy (Pryor *et al* 2006), the insurance sector (Sparks *et al* 1994), air pollution dispersion (McVicar and Roderick 2010), dust storms (Cowie *et al* 2013,

Fan *et al* 2014), extreme temperatures (Horton *et al* 2015) and wind-related hazards and catastrophes (Kim and Paik 2015). For example, one of the most direct impacts of stilling is on long-term wind power industry that is rapidly developing and requires large infrastructural investments. So far, the drivers and physical mechanisms behind terrestrial stilling have not been determined, and thus it is unclear whether the observed stilling will continue (Vautard *et al* 2010, Peterson *et al* 2011, McVicar *et al* 2012b, Wu *et al* 2018).

Decreasing *u* over land can be attributed to the driving force (i.e. a change in large-scale atmospheric circulation) and/or the drag force (i.e. an increase in surface roughness associated with land surface change). If the trend in *u* is mainly driven by changes in the force term, the decrease in *u* should be observable over both land and ocean and should also be present in climate reanalysis products (Pryor *et al* 2009, Vautard *et al* 2010). However, satellite altimeter measurements show a widespread increase of *u* over the ocean (Wentz *et al* 2007, Young *et al* 2011). Neither NCEP/NCAR nor ECMWF ERA-interim reanalysis products produce any trend in *u* over land (McVicar *et al* 2008, Pryor *et al* 2009, Vautard *et al* 2010). Therefore, the terrestrial stilling was hypothesized to be due to an increasing drag force on the atmosphere from the land surface, rather than a decreasing driving force (Vautard *et al* 2010).

One of the most widespread changes in the Earth's land cover is the enhanced vegetation growth during the past several decades, which is observed from satellites as the greening of the Earth (Zhu *et al* 2016). The global vegetation leaf area index (LAI, as a proxy for land greening) has enhanced by 8% during the past 30 years as indicated by satellite-observations (Zhu *et al* 2013, 2016). The greening is particularly large over middle to high latitudes in the Northern Hemisphere (Myneni *et al* 1997, Xu *et al* 2013, Zhu *et al* 2016), where terrestrial stilling is observed (McVicar *et al* 2008, 2012a, 2012b). Enhanced vegetation LAI is associated with increased primary productivity and biomass, including tree height. Depending upon carbon allocation, an increment of net primary productivity is redistributed among root, stem and trunk. The latter will increase plant height and also surface roughness, which can decrease *u*. Vautard *et al* (2010) found a significant and negative spatial correlation between increased vegetation greenness (spring-summer normalized difference vegetation index (NDVI) trend) and stilling (*u* trend) across the stations in the Northern Hemisphere. They hypothesized that the cause of the terrestrial stilling could be an increase in surface roughness associated with enhanced vegetation activity, but NDVI is not directly related to LAI, and saturates with biomass. Further, NDVI can also change from vegetation structural shifts like the development of shrubs, as observed in dry regions and Arctic tundra (Frost and Epstein 2014, Tape *et al* 2006).

More importantly, correlation does not imply causation. The correlation could be derived from measuring a linear relationship due to factors that have nothing to do with NDVI and *u*. The role of enhanced vegetation growth (the greening of the Earth) in the terrestrial stilling remains unknown. The objective of this study is to test whether enhanced vegetation growth contributed to the terrestrial stilling observed over the past decades. This question is addressed by combining *in situ* and satellite observations of winds together with simulations of coupled land-atmosphere models.

In this study, we first examine the extent and patterns of changes in *u* during the period 1982–2011 using records from *in situ* meteorological stations over land and long-term satellite-derived observations over the ocean (Wentz *et al* 2007, Remote Sensing Systems 2015). We selected 4305 *in situ* stations that have more than 20 years of wind records from 26 247 meteorological stations (Global Surface Summary of the Day—GSOD). To isolate the wind response to changes in LAI, we ran two state-of-the-art coupled land-atmosphere models (the Community Earth System Model, CESM (Hurrell *et al* 2013) and the Institut Pierre Simon Laplace Coupled Model, IPSLCM (Marti *et al* 2010)) forced with satellite-observed LAI over a 30 years period (1982–2011). Note that LAI controls photosynthetic primary production, and is a key variable impacting vegetation growth in all models. We performed ensemble decadal Atmospheric Model Intercomparison Project (AMIP)-type simulations to make sure that the simulated climate is comparable with the historical climate (He and Soden 2016). The accuracy of the CESM and IPSLCM simulations in reproducing the historical climate change and the biophysical climatic feedbacks was evaluated by Zeng *et al* (2017, 2018a).

2. Methods

2.1. Observations

Satellite-derived observations of monthly average *u* over the ocean were obtained from the RSS V7 DISCOVER microwave radiometer data set on a 1° grid for the period 1988–2011 (Wentz *et al* 2007, Remote Sensing Systems 2015). The satellite microwave radiometer, including SSM/I F08 through F15, SSMIS F16 and F17, WindSat, and AMSR2, are first inter-calibrated at the brightness temperature level, and are then used to construct the merged, 1° wind speed data set using a consistent processing methodology for all sensors (Remote Sensing Systems 2015). This data set has been carefully inter-calibrated and consistently processed. The *in situ* measurements of *u* (at 10 m height) over land were obtained from the GSOD (ftp://ftp.ncdc.noaa.gov/pub/data/gsod). This meteorological dataset is produced by National Centers for Environmental Information (NCEI) and includes 26 247 *in situ* stations based on the data

exchanged under the World Meteorological Organization World Weather Watch Program. NCEI eliminated random errors in the original data, and performed extensive automated quality control. For this analysis, we only selected stations with more than 20 years of wind records during the period of 1982–2011. In determining whether a year of data is available, monthly mean u was calculated if more than 50% of the days in a month were available, and annual mean u was calculated only if all the months in the year were available. As a result, a total of 4305 meteorological stations over continents were selected.

Current climate models simulations are very uncertain, particularly at regional scales, partly as a result of sea surface temperature and sea ice (SST) biases in coupled ocean-atmosphere models (He and Soden 2016). To improve the projections of anthropogenic climate change, we performed simulations with the land-atmosphere coupled models forced with observed SST during the past several decades. We obtained SST data for the period of 1982–2011 from the AMIP (http://pcmdi.llnl.gov/projects/amip/). This is a dataset grounded on observations and widely used in the AMIP-type simulations. There are significant increasing trends (significant level, $p < 0.05$) of SST over most of the ocean except for the tropical Pacific Ocean and the Southern Ocean (figure S1(a) is available online at stacks.iop.org/ERL/13/124013/mmedia). Overall, global SST significantly increased by 0.09 °C per decade during the study period ($p < 0.01$).

The greening of the Earth is represented by LAI observations from satellites (Zhu *et al* 2016). Monthly LAI was obtained from the advanced very high resolution radiometer 8 km global LAI product, which is derived from the third generation GIMMS NDVI3g from 1982 to 2011 (Zhu *et al* 2013). During the past 30 years, global land LAI has increased significantly by 8%, dominated by growth in the Amazon rainforest, the Sahel, Eurasian boreal forests, Europe, India, the eastern United States and southern China (figure S1(b)).

2.2. Numerical experiments

We performed several simulations with an ensemble of variable initial conditions using two state-of-the-art ESMs: the IPSLCM (version 4) from the Institute Pierre Simon Laplace at France (Marti *et al* 2010), and the CESM (version 1.3) from the National Center for Atmospheric Research at United Sates (Hurrell *et al* 2013). The horizontal spatial resolutions of IPSLCM and CESM are $3.75° \times 2.5°$ and $1.875° \times 2.5°$, respectively, while the time step is 1.5 min. The methodology follows Zeng *et al* (2017, 2018a), where details of the simulation protocols can be found in the methods section and the supplementary information.

We conducted two 30-year long AMIP-style experiments (AMIP_STD and AMIP_LAI) with the

two models. Both experiments are constrained by observed SST from 1982 to 2011. In addition, while the LAI in AMIP_STD is forced with climatological monthly values, AMIP_LAI uses observed monthly LAI maps from 1982 to 2011. To reduce the uncertainty due to initial conditions (Lorenz 1963, Daron and Stainforth 2013), all experiments contain a large ensemble with different initial conditions ($n = 30$ for both models). The initial conditions of all realizations are identical, derived from a model output of an unperturbed 60 years run. The ensemble average was then used to characterize the response of u to prescribed changes in SST and LAI.

Surface u at 10 m was extracted from the model simulations. Similar to the reality, u is dependent upon drive and drag forces in the models. The drive term is pressure gradient force primarily owing to the simulated heterogeneity of temperature. It drives u over both the ocean and land surfaces. The drag term is caused by surface roughness associated with land surface characteristics. The drag term is negligible for u over the ocean, but not over land. SST change drives changes in climate (Kosaka and Xie 2013, He and Soden 2016), causing warming gradient that changes pressure gradient and u over land. LAI change has effects on both force and drag terms. On one hand, it triggers changes in land surface air temperature (Zeng *et al* 2017). The LAI-induced cooling has heterogeneity and this will superimpose on the force term.

On the other hand, surface roughness, similar to surface albedo, is computed from the simulated/prescribed state of the vegetation. Generally, models use LAI to represent vegetation growth and calculate photosynthetic primary production. Increased biomass is redistributed to root, stem and trunk, and is further used to calculate tree height. The simulated height of trees is then used to compute surface roughness (Su *et al* 2001), which influences the drag term. Below we take the land surface model in IPSLCM (details see Krinner *et al* 2005) as an example. As for photosynthesis at the canopy level, the assimilation rate (A_c) is integrated with LAI:

$$A_c = \int_0^{\mathrm{LAI}} A_n(l)\,\mathrm{d}l, \tag{1}$$

where l is the cumulative LAI, A_n is assimilation at the leaf level. Thus enhanced LAI increases photosynthetic primary production and carbon assimilation, which is further allocated to the biomass in different compartments (e.g. leaves, stems, roots, fruits) based on the allocation scheme in the model.

The simulated biomass in the wood (B_m) is further used to calculate the wood's diameter (D):

$$D = \left(\frac{B_m}{\pi p_1 / 4}\right)^{\frac{1}{2 + p_2}}, \tag{2}$$

where π is the ratio of a circle's circumference to its diameter, p_1 is a parameter relevant to pipe density (40, dimensionless), p_2 is a tune parameter relevant to

pipe (0.5, dimensionless). The equation for D and the behind parameters are developed based on the pipe model theory (Shinozaki *et al* 1964). D is further used to calculate vegetation height (H):

$$H = p_3 D^{p_2}, \qquad (3)$$

where p_3 is a tune parameter relevant to pipe (0.3, dimensionless).

Finally, the surface roughness length (z_0) is calculated based on the simulated vegetation height and vegetation fractions:

$$z_0 = \exp\left(\frac{1 - \sum\limits_{\text{nobio}} F_{\text{nobio}}}{F_{\text{bare}} \ln(z_{0\_\text{bare}}) + \sum\limits_{\text{PFT}} F_{\text{PFT}} \ln(\max(z_{0\_\text{oh}} H_{\text{PFT}}, z_{0\_\text{bare}}))} + \sum\limits_{\text{nobio}} F_{\text{nobio}} \ln(z_{0\_\text{nobio}})\right), \qquad (4)$$

where H_{PFT} is vegetation height for each PFT, z_{0_oh} is a parameter to get z_0 from height of canopy (0.0625, dimensionless), z_{0_bare} is bare soil roughness length (0.01 m), z_{0_nobio} is roughness length for other non-vegetation surface types (e.g. ice, lake, ocean; nobio is the number of the types) (0.001 m), F_{PFT} is vegetation fraction for each PFT, F_{bare} is fraction for bare ground, F_{nobio} is fraction for each non-vegetation surface types.

3. Results and discussion

3.1. Trend in observed *u* over land
Over land, mean annual *u* across all selected stations (4305 sites) significantly declined by on average -0.07 m s^{-1} per decade, or 5.8% during 1982–2011 ($p < 0.01$; figures 1(a), (b)). Interestingly, mean annual global *u* was relatively stable during the 1980s and then steadily decreased during the following two decades. Spatially, as shown in figure 1(a), most of the stations with decreasing *u* were located in the northern mid-latitudes, including North America (599 of 941 stations, 64%), Europe (843 of 1283 stations, 66%), Central Asia (307 of 398 stations, 77%), Eastern Asia (364 of 606 stations, 60%) and India (44 of 55 stations, 80%). On average, the decreasing rates over these regions are -0.07 m s^{-1} per decade (North America, figure 1(c)), -0.06 m s^{-1} per decade (Europe, figure 1(d)), -0.18 m s^{-1} per decade (Central Asia, figure 1(e)), -0.03 m s^{-1} per decade (Eastern Asia, figure 1(f)) and -0.20 m s^{-1} per decade (India, figure 1(g)). In North America and Europe, decreasing *u* primarily occurred during the last two decades (figures 1(c) and (d)). In Central Asia and India, the rapid decrease of *u* occurred during the first two decades and the decreasing rate slowed down during the last decade (figures 1(e) and (g)). Meanwhile, in Eastern Asia, mean annual *u* increased during the first two decades, and then decreased during 2002–2011 (figure 1(f)). The widespread decreasing *u* at the
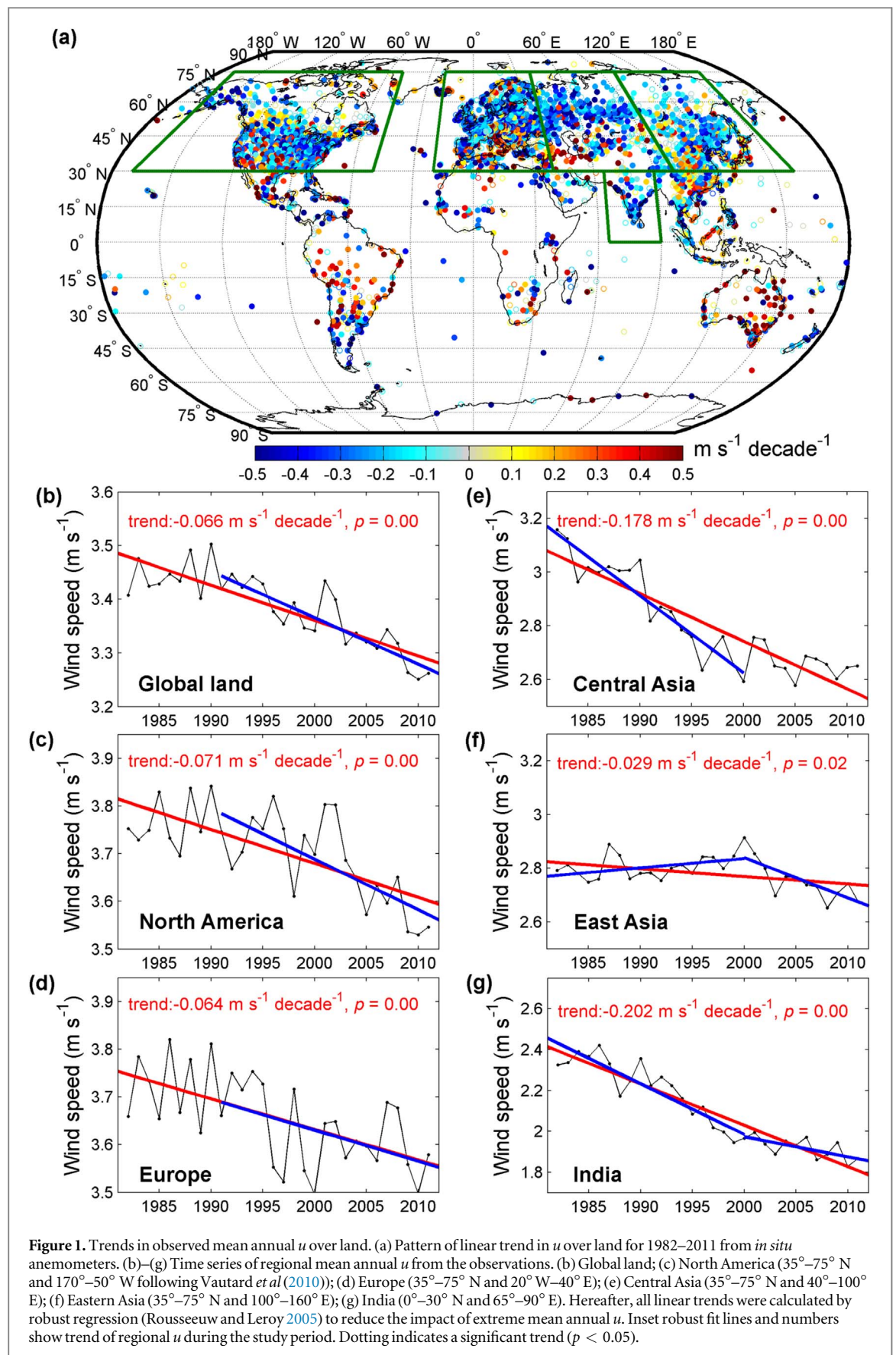
surface over the northern mid-latitudes during the past 30 years is documented in several studies (e.g. Vautard *et al* 2010, McVicar *et al* 2012b). There are fewer stations in other regions, in particular the tropics and the Southern Hemisphere (figure 1(a)). It is thus difficult to conclude the wind speed change over these regions.

Overall, the trends in *u* for the four seasons follow similar patterns with those in mean annual *u* (figures 2 and S2). During the past three decades, mean *u* averaged over all weather stations significantly declined by -0.070 m s^{-1} per decade ($p < 0.01$) in MAM (March, April, and May), 0.047 m s^{-1} per decade ($p < 0.01$) in JJA (June, July, and August), 0.073 m s^{-1} per decade ($p < 0.01$) in SON (September, October, and November), and 0.077 m s^{-1} per decade ($p < 0.01$) in DJF (December, January, and February), respectively. The rapidest decline in *u* occurred during SON in North America (0.090 m s^{-1} per decade, $p < 0.01$; figure 2(b3)), during DJF in Europe (0.107 m s^{-1} per decade, $p < 0.01$; figure 2(c4)), during DJF in Central Asia (0.227 m s^{-1} per decade, $p < 0.01$; figure 2(d4)), during JJA and SON in Eastern Asia (0.050 m s^{-1} per decade, $p < 0.01$; figures 2(e2) and (e3)), and during JJA in India (0.172 m s^{-1} per decade, $p < 0.01$; figure 2(f2)). The reason why the declines of *u* in North America, Europe and Eastern Asia are much weaker than that in Central Asia and India is that there are more stations with positive trends in *u* in these regions (figure S2). For example, many stations surrounding the Mediterranean show positive trends in *u* during the period 1982–2011 (figure S2), making a relative weak trend in *u* averaged over Europe (figure 2). During JJA, the trend in *u* averaged over Europe is even non-significant ($p = 0.56$, figure 2(c2)).

3.2. Modelled response of *u* over ocean and land to SST changes
To isolate the climate response of *u* to the greening of the Earth, we ran the CESM and IPSLCM models forced with observed SST and variable/climatological LAI. We first tested the ability of the models to represent the response of *u* to SST-driven climate change. Note that simulated climate change driven by SST change compares well with the historical spatial-temporal variations in precipitation, temperature and evapotranspiration, as shown in Zeng *et al* (2018a, figures S3–5 in the paper). The DISCOVER satellite-retrieved *u* field over oceans during the past decades (Wentz *et al* 2007) is used to evaluate *u* trends. According to the DISCOVER observations, there is a

Figure 1. Trends in observed mean annual *u* over land. (a) Pattern of linear trend in *u* over land for 1982–2011 from *in situ* anemometers. (b)–(g) Time series of regional mean annual *u* from the observations. (b) Global land; (c) North America ($35°–75°$ N and $170°–50°$ W following Vautard *et al* (2010)); (d) Europe ($35°–75°$ N and $20°$ W–$40°$ E); (e) Central Asia ($35°–75°$ N and $40°–100°$ E); (f) Eastern Asia ($35°–75°$ N and $100°–160°$ E); (g) India ($0°–30°$ N and $65°–90°$ E). Hereafter, all linear trends were calculated by robust regression (Rousseeuw and Leroy 2005) to reduce the impact of extreme mean annual *u*. Inset robust fit lines and numbers show trend of regional *u* during the study period. Dotting indicates a significant trend ($p < 0.05$).

widespread negative trend in *u* over the Western Pacific and the Northern Atlantic (figure S3(a)). This is in line with previous studies that documented a decreasing *u* al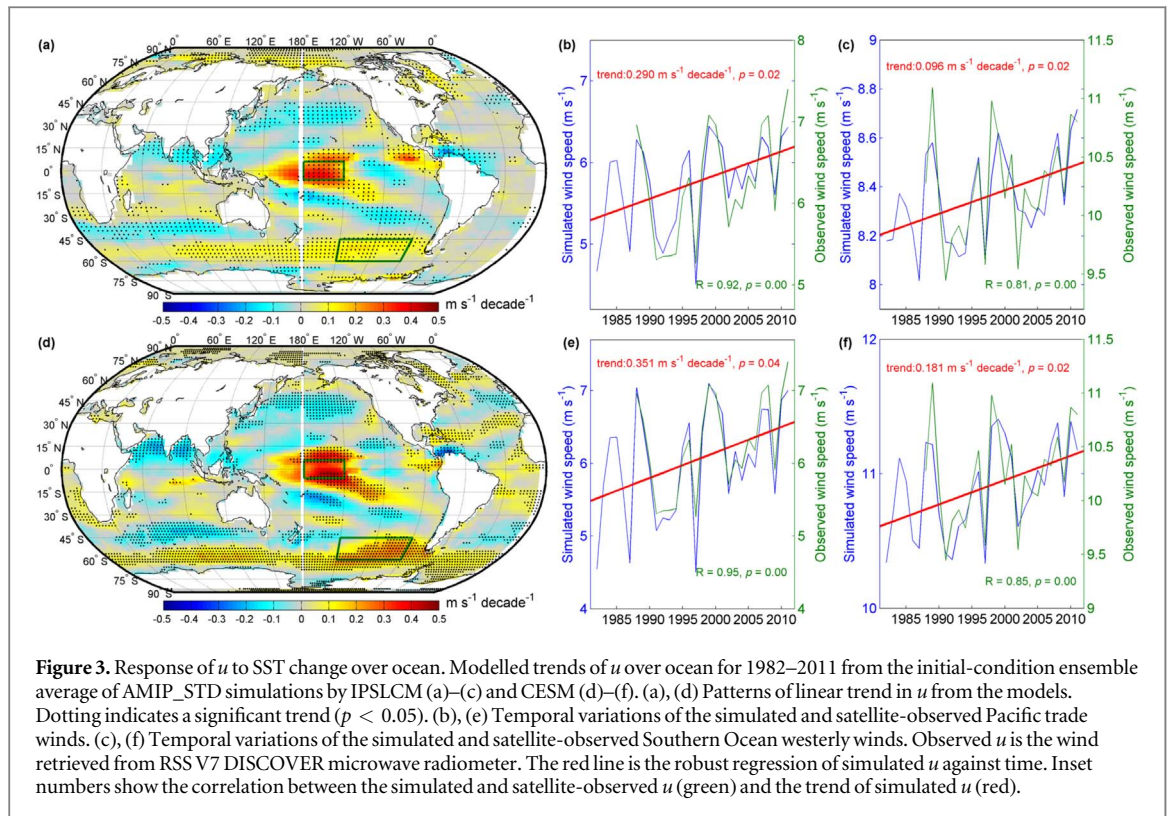ong with weakening circulation under global warming (Held and Soden 2006, Vecchi and Soden 2007). However, strongly positive trends in *u* are observed over the Central Pacific and for the Southern Ocean westerly winds (figure S3(a)). Averaged over

Figure 2. Time series of observation-based regional *u* for the four seasons: (1) boreal spring (MAM; March, April and May), (2) boreal summer (JJA; June, July and August), (3) boreal autumn (SON; September, October and November), and (4) boreal winter (DJF; December, January and February). (a1)–(a4) Global land; (b1)–(b4) North America; (c1)–(c4) Europe; (d1)–(d4) Central Asia; (e1)–(e4) Eastern Asia; (f1)–(f4) India. Inset robust fit lines and numbers show trend of regional *u* during the study period.

all the oceans, there is no significant trend in annual *u* during the period 1988–2011 (figure S3(b)). However, Central Pacific trade winds significantly increased at a rate of $0.41 \, \text{m s}^{-1}$ per decade, while the Southern Ocean westerly winds increased by $0.22 \, \text{m s}^{-1}$ per decade. Both trends mainly occur during 1992–2011 ($p < 0.05$; figures S3(c), (d)). It has been reported that the increasing wind over this region has a profound effect on global climate, as it is suspected to be the cause of the recent warming hiatus (Kosaka and Xie 2013, England *et al* 2014).

The simulations showed that SST-forced *u* is generally decreasing in regions where SST are increasing, and increasing in the regions where SST are decreasing (figures 3(a), (d)). Spatially, SST increased over the entire ocean with the exception of the Eastern Pacific and Southern Ocean (figure S1(a)). Significant decreasing *u* is found over the western Pacific Ocean, the Indian Ocean, the Equatorial Atlantic and the Western North Atlantic, where SST have warmed during the past decades (figures 3(a), (d)). In contrast, SST

over the Eastern Pacific and Southern Ocean has been decreasing. Both models simulate increasing *u* over these regions. Interestingly, although the warming rate is much greater than the cooling rate (figure S1(a)), the strengthening of *u* where SST decreased is much stronger than the weakening of *u* where SST increased (figures 3(a), (d)). Comparing modelled *u* with satellite-observed *u*, the pattern of the trends of *u* over the ocean are well reproduced by the models, particularly the strengthening of the Pacific trade winds (figures 3(b), (e)) and Southern Ocean westerly winds (figures 3(c), (f)). For the Pacific trade winds (figures 3(b), (e)), the modelled regional trend of *u* is $0.32 \pm 0.04 \, \text{m s}^{-1}$ per decade for the period of 1982–2011 ($0.30 \pm 0.04 \, \text{m s}^{-1}$ per decade for 1988–2011), which is similar to the observed trend ($0.41 \, \text{m s}^{-1}$ per decade for 1988–2011). Moreover, the interannual variation of modelled *u* is significantly correlated with observed *u* (correlation coefficient, $R = 0.92$ and 0.95 for IPSLCM and CESM, all with $p < 0.01$, figures 3(b), (e)). In addition, both models

Figure 3. Response of *u* to SST change over ocean. Modelled trends of *u* over ocean for 1982–2011 from the initial-condition ensemble average of AMIP_STD simulations by IPSLCM (a)–(c) and CESM (d)–(f). (a), (d) Patterns of linear trend in *u* from the models. Dotting indicates a significant trend ($p < 0.05$). (b), (e) Temporal variations of the simulated and satellite-observed Pacific trade winds. (c), (f) Temporal variations of the simulated and satellite-observed Southern Ocean westerly winds. Observed *u* is the wind retrieved from RSS V7 DISCOVER microwave radiometer. The red line is the robust regression of simulated *u* against time. Inset numbers show the correlation between the simulated and satellite-observed *u* (green) and the trend of simulated *u* (red).

similarly reproduced the interannual variation in satellite-observed Southern Ocean westerly winds and their trends (figures 3(c), (f)). The satellite observations of *u* over the oceans are only available from 1988 onwards. The simulated long time series (figure 3) clearly shows that there are anomalies in the Pacific trade winds during 1982–1996. The strengthening of Pacific trade winds began in 1997, corresponding to the ongoing warming hiatus.
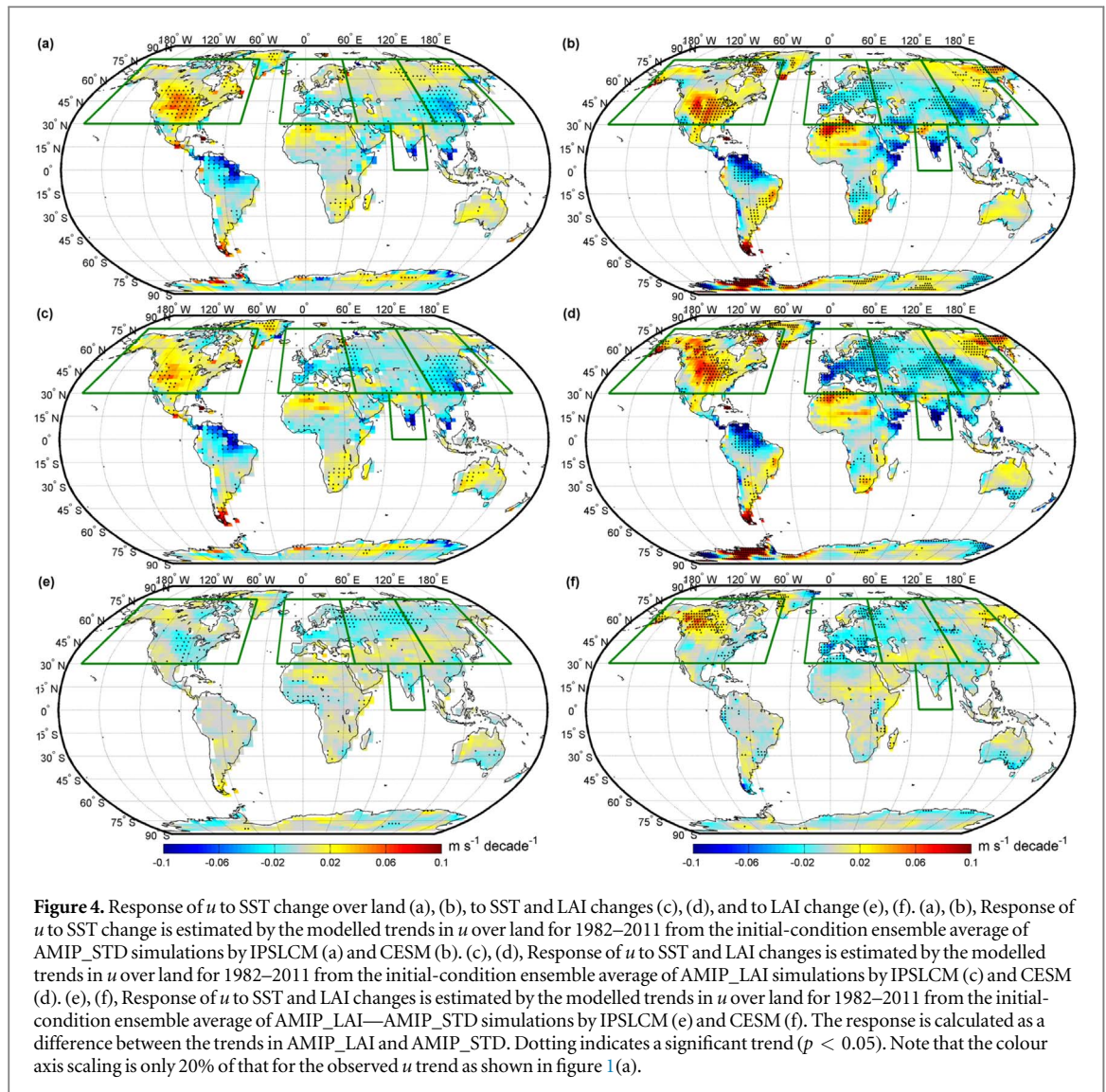
Combined with previous findings that the tropical Pacific cooling is a result of the unprecedented strengthening in Pacific trade winds (England *et al* 2014) and the results from this study that SST trends explain the strengthening in Pacific trade winds, we hypothesize the existence of a strong positive coupling between SST and Pacific trade winds. The positive feedback indicates that the climate system is sensitive to initial conditions (Lorenz 1963) over this region (approximately Nino 3.4 region): the strengthening in Pacific trade winds cools the ocean SST in the eastern Pacific and pushes the warm pool to the west, which reinforces Pacific trade winds and further cools the ocean SST in the eastern Pacific; globally, the cooling over this region feeds back to the global climate system and has led to the recent ongoing warming hiatus (Kosaka and Xie 2013).

If, like that of the change in *u* over the oceans, the change in *u* over land is driven by the global circulation change, the historical observations of *u* change over land should be reproduced by the SST-driven model simulations as well. However, in both model simulations (IPSLCM and CESM, static LAI simulations), the magnitude of the SST-forced *u* trend for the

last 30 years is an order of magnitude smaller than the observed (negative) *u* trend over land (figures 4(a), (b) versus figure 1(a)). While the sign of SST-forced *u* trend is consistent with the observed *u* trend over Eurasia and India (negative trend), it is opposite to the observed *u* trend over North America (widespread positive trend; figures 4(a), (b) versus figure 1(a)). Similar results are found in the NCEP/NCAR and the ECMWF ERA-interim reanalysis products: the observed *u* trends over ocean have been well captured, while that over the northern mid-latitudes was not (figures S4–5) (Kalma *et al* 2008, Pryor *et al* 2009, Vautard *et al* 2010). According to these model results, the SST-driven circulation change seems not a determinant for the global terrestrial stilling. We note, however, more details about the model uncertainty should be investigated in future.

3.3. Modelled response of *u* over land to the greening of the Earth
Next, we tested the hypothesis that increase of LAI contributed to the stilling. If this hypothesis is valid, forcing the models with the observed LAI change in addition to SST should reproduce the *in situ* observed surface *u* change over land. However, even though the models are constrained by both observed LAI and SST, there are substantial discrepancies between the modelled trend in *u* (figures 4(c), (d)) and the observed trend in *u* over land (figure 1(a)). We isolated the contribution of LAI trends to *u* change over land from the difference (Δ) between ensemble simulations with observed LAI change (AMIP_LAI) and climatological

Figure 4. Response of *u* to SST change over land (a), (b), to SST and LAI changes (c), (d), and to LAI change (e), (f). (a), (b), Response of *u* to SST change is estimated by the modelled trends in *u* over land for 1982–2011 from the initial-condition ensemble average of AMIP_STD simulations by IPSLCM (a) and CESM (b). (c), (d), Response of *u* to SST and LAI changes is estimated by the modelled trends in *u* over land for 1982–2011 from the initial-condition ensemble average of AMIP_LAI simulations by IPSLCM (c) and CESM (d). (e), (f), Response of *u* to SST and LAI changes is estimated by the modelled trends in *u* over land for 1982–2011 from the initial-condition ensemble average of AMIP_LAI—AMIP_STD simulations by IPSLCM (e) and CESM (f). The response is calculated as a difference between the trends in AMIP_LAI and AMIP_STD. Dotting indicates a significant trend ($p < 0.05$). Note that the colour axis scaling is only 20% of that for the observed *u* trend as shown in figure 1(a).

LAI (AMIP_STD) (figures 4(e), (f)). Globally, ΔLAI induces *u* changes that are significantly negatively correlated to interannual variation of LAI for 1982–2011 in both IPSLCM ($R = -0.47$, $p < 0.01$; figure 5(a1)) and CESM ($R = -0.53$, $p < 0.01$; figure 5(b1)), indicating that ΔLAI induced a decreasing trend in global surface land *u* of -0.006 m s^{-1} during the period. This LAI explained stilling trend (-0.006 m s^{-1}) is an order of magnitude smaller than the observed trend from *in situ* observations (-0.198 m s^{-1}, figure 1(b)).

As described in the Method (2.2), the greening of the Earth impacts on *u* over land through two mechanisms: (1) it triggers temperature heterogeneity and induces changes in pressure gradients; (2) it increases surface roughness length (z_0) and the drag force, which slows down *u* over land. To estimate the LAI-induced change in z_0, we extracted the modelled z_0 from two equilibrium simulations (Zeng *et al* 2018a) which are two 60-year long simulations that share the same setup but are forced by different seasonal LAI maps (the 1980s: the average observed from

1982 to 1986 versus the 2010s: the average observed from 2007 to 2011). While the relative change of LAI is 8% between the 1980s and 2010s, the modelled relative change in z_0 is only 1.3%, changing from 0.2569 in the 1980s to 0.2601 in the 2010s. Assuming an unchanged pressure gradient, the change in z_0 leads to 0.35% decrease of surface wind speed at 10 m height (Kelly and Jørgensen 2017), which is -0.013 m s^{-1} during 1982–2011. It is still an order of magnitude smaller than the observed trend from *in situ* observations (-0.198 m s^{-1}, figure 1(b)).

Spatially, as shown in figures 4(e)–(f), modelled significant decreasing *u* occurs in the regions where LAI is significantly increasing (figure S1(b)), including Europe, Central Asia, India, Southern China, Eastern United States and Southern Australia. There is no robust signal of the modelled response of *u* to greening in North America (-0.003 m s^{-1} per decade in IPSLCM and 0.012 m s^{-1} per decade in CESM; figures 5(b1), (b2)). In Europe, CESM produces a significant decrease of regional *u* as a response to ΔLAI at a rate of -0.018 m s^{-1} per decade ($p < 0.01$,
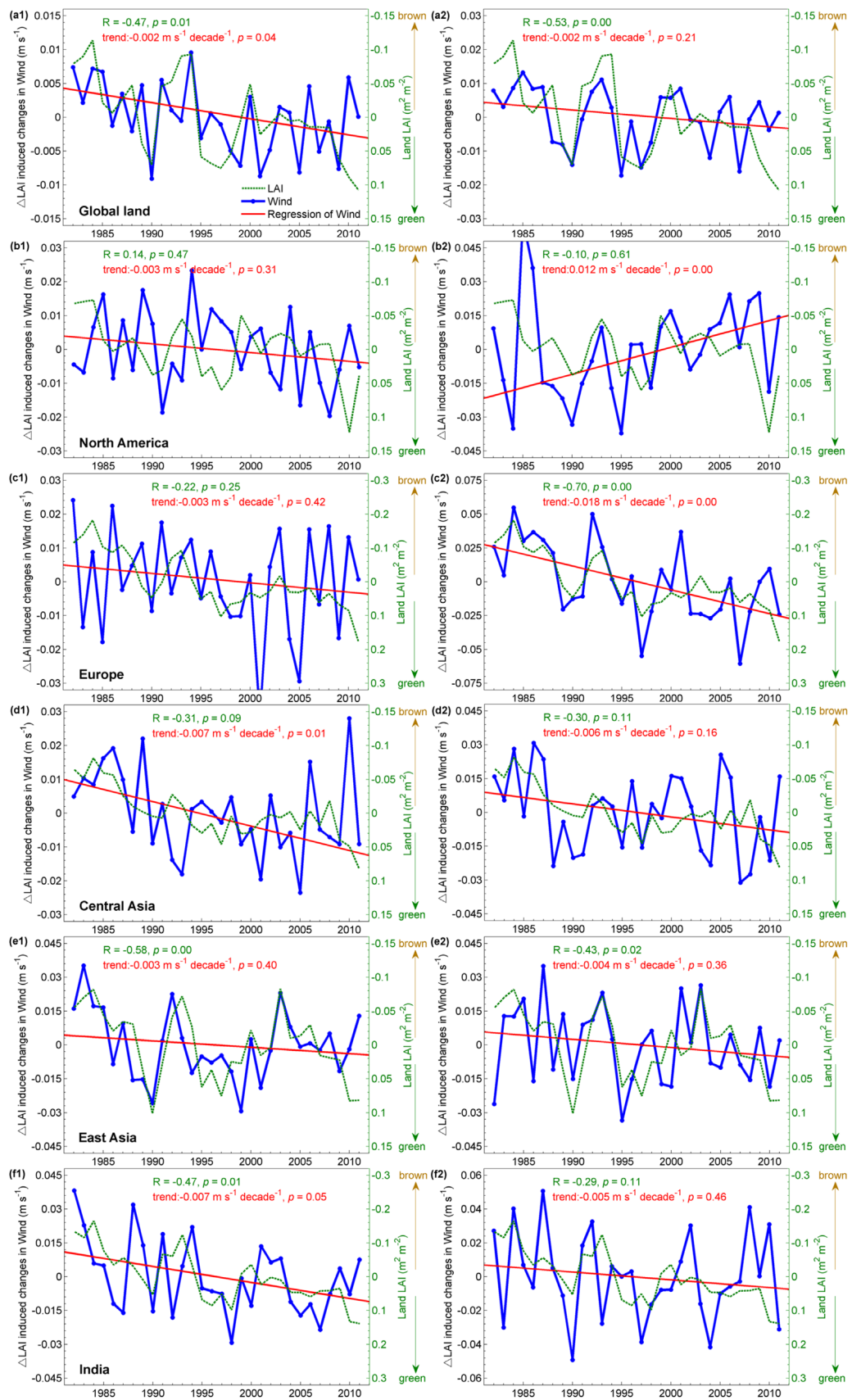
Figure 5. Time series of regional mean annual *u* from the AMIP_LAI-AMIP_STD simulations by (1) IPSLCM and (2) CESM. (a) Global land; (b) North America; (c) Europe; (d) Central Asia; (e) Eastern Asia; (f) India. The green line is the satellite-derived mean annual LAI over the regions. The red line is the robust regression of the simulated *u* against time. Inset numbers show the correlation between the simulated *u* and LAI (green) and the trend of simulated *u* (red).

figure 5(c2)), which is 28% of the observed stilling in this region (figure 1(d)). In Central Asia, both IPSLCM and CESM produced a decrease in regional u as a response to ΔLAI (-0.007 m s^{-1} per decade; only 4% of the observed stilling in the region). In East Asia, there is no significant LAI driven trend in u in the simulations of both models ($p > 0.05$; figures 5(e1), (e2)). In India, IPSLCM produced a significant decrease in regional u as a response of ΔLAI, but the rate is only 3% of the observed decrease in the region.

Therefore, the simulations indicate that the modelled responses of u to the greening remain orders of magnitude smaller than the observed u trends over land. It rejected the hypothesis that the greening of the Earth is a driver of the global terrestrial stilling. Model simulations depends strongly on how roughness is parameterized as a function of LAI in land surface models and how good is their aerodynamic coupling with the atmosphere. Given the large uncertainties behind the parameterization and the processes in the model, we examined this model results with more analyses directly based on the observations (see next section).

3.4. More evidence based on the coherence between the observed changes in u and LAI

The spatial coherence between satellite greenness (NDVI) and stilling over the middle to high latitudes in the Northern Hemisphere is a reason why we hypothesized that the greening is a determinant of the terrestrial stilling (also see Vautard *et al* 2010). Temporally, we did find a significant correlation between mean annual u and LAI averaged over the boreal Northern Hemisphere (north 30°) for the period 1982–2011 ($R = -0.53$, $p < 0.01$). But this is an apparent correlation as it becomes non-significant when both time series are detrended ($R = 0.15$, $p = 0.44$). Furthermore, the correlation coefficients between detrended regional averaged u and LAI over all the individual regions with sufficient *in situ* stations are not significant (all with $p > 0.05$; e.g. North America, $p = 0.86$; Europe, $p = 0.54$; Central Asia, $p = 0.20$; East Asia, $p = 0.62$; and India, $p = 0.95$). Even for the long-term trend, the northern mid-high latitudes have been greening from 1981 to 1999 (Myneni *et al* 1997), yet during this period, mean annual u did not decrease over North America (figure 1(c)) and Europe (figure 1(d)), both with p-value higher than 0.05. In East Asia, while the region-average LAI significantly increased for 1982–1999 ($p < 0.05$; figure S1(b)), the region-average u is increased rather than decreased during the same period (0.035 m s^{-1} per decade, $p = 0.06$; figure 1(f)).
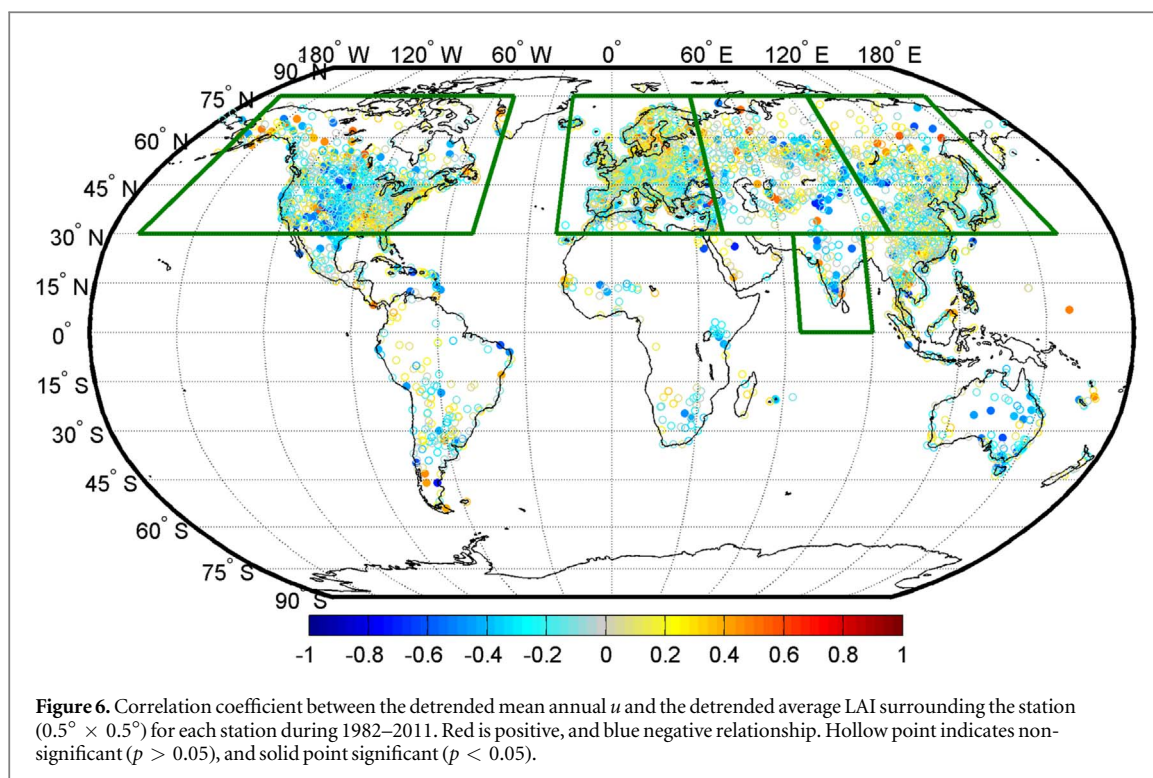
Furthermore, the coherence between LAI and u trends does not exist everywhere if we examine it at a finer scale. For example, vegetation surrounding the Mediterranean is greening but u observed by many stations in this region is increasing during the past

decades (figures S1(b) and 1(a)). In southern China and Japan, vegetation is greening but u is also increasing. Vegetation is browning (LAI decrease) in southern Alaska, central Canada and northern Russia, yet u in these regions is decreasing rather than increasing (figures S1(b) and 1(a)). In addition, if the surface stilling was mainly caused by the greening, the stilling should be larger in the growing season over deciduous forests. However, the observed decline of u in DJF (boreal winter) is 64% more than the decline in JJA (boreal summer). The rapidest decline in u occurred in Central Asia during boreal winter where and when widespread browning rather than greening is dominated (figures 2(d4), S6(d)). This decreasing rate (-0.227 m s^{-1} per decade, $p < 0.01$) is much more than that in any other region and during any other seasons. Although widespread greening has occurred over Europe during the boreal summer (JJA; figure S6(b)), there is no significant trend in u averaged over Europe during this season ($p = 0.56$, figure 2(c2)).

Lastly, if the terrestrial stilling is mainly caused by an increase in surface roughness associated with the local vegetation change, there should be a significant correlation between the u observed by *in situ* station and LAI surrounding the station for the past decades (1982–2011). However, we found no significant correlation between the detrended mean annual u and the detrended average LAI surrounding each station ($0.5° \times 0.5°$) at the majority of the stations (3842/ 4305, 89%; figure 6). These results support the simulation results that the greening is not a dominant driver of the terrestrial stilling during the past decades.

3.5. Caveat and future studies to attribute the terrestrial stilling

Models are imperfect, resulting in uncertainties in model simulations. As for the LAI-induced change in driving force, models are required to accurately simulate the responses of evapotranspiration and albedo, so that changes in air temperature and air pressure gradient can be reproduced by the models. However, because of systematic error in evapotranspiration partitioning, the CESM model failed to represent the response of evapotranspiration to the greening (Zeng *et al* 2017), and thus the simulated u change is uncertain. As for the LAI-induced change in drag force, models are supposed to correctly simulate the response of plant height to LAI change via vegetation grow models, and also the response of surface roughness to plant height change based on boundary theories. Yet, we cannot evaluate the responses of plant height and surface roughness to LAI change owing to the lack of global observations of plant height change and surface roughness. Regional long term measurements of plant height and surface roughness will be useful to evaluate the roughness parameterization in the model, and to reduce the uncertainty in attributing the terrestrial stilling to

Figure 6. Correlation coefficient between the detrended mean annual u and the detrended average LAI surrounding the station $(0.5° \times 0.5°)$ for each station during 1982–2011. Red is positive, and blue negative relationship. Hollow point indicates non-significant ($p > 0.05$), and solid point significant ($p < 0.05$).

changes in surface land cover. Last, while the uncertainties exist in the model simulations, the results are supported by several evidence based on the coherence analyses between the observed changes in u and LAI (see the section 3.3).

Another caveat is that the large scale deforestation (e.g. Southeast Asia during 2000–2014 (Zeng *et al* 2018b)) has not been considered in this study. Large-scale deforestation may intensify rather than weaken u, as it leads to a decrease of surface roughness. However, surface roughness could increase due to the deforestation induced forest fragmentation (Taubert *et al* 2018), and thus deforestation may also weaken u depending on its spatial pattern. Current high-resolution satellite observations of land cover change make it possible to detect historical change in forest fragmentation (e.g. Taubert *et al* 2018; Zeng *et al* 2018c). Yet, the current model horizontal resolution may be not fine enough to characterize the heterogeneous nature of the landscape (e.g. regional deforestation and forest fragmentation). In addition, fluffy cumulus clouds may act like anchors to create drag and slow the winds. But they are too small to register on the resolution for current climate models (Nuijens *et al* 2018). Future study using higher-resolution models could resolve the issue whether finer characterizations of land surface and/or clouds is an important element of the wind stilling.

4. Conclusion

We evaluated the global trend in u with 4305 *in situ* meteorological observations over land for the period 1982–2011, and the long-term satellite altimeter measurements over ocean for the period 1988–2011. The results presented here are consistent with previous results of a widespread negative trend in u over land, particularly the northern mid-latitudes, and a profound positive trend in u over Central Pacific Ocean and Southern Ocean. To isolate the response of u to the greening of the Earth for 1982–2011, we performed ensemble decadal AMIP-type simulations by prescribing the observed LAI and SST in two state-of-the-art ESMs (IPSL-CM and CESM). The SST-driven global circulation change can fully explain the observed change in u over the ocean, specifically the strengthening of Pacific trade winds and Southern Ocean westerly winds, proving the ability of the models to represent the response of u to climate change. The simulations showed that SST-driven global circulation change can partly explain the stilling over the Eurasia, but not North America. As for the u response to greening, regionally, the greening in Europe can explain 28% of the observed decrease in u over the region. However, globally, increasing LAI during the last 30 years (+8%) can only explain in the two models formulations to a decrease of terrestrial u by -0.006 m s^{-1}, an order of magnitude smaller than the observed trend from *in situ* stations (-0.198 m s^{-1}). Therefore, the simulations by both models reject the hypothesis that the greening of the Earth is a key driver of the global terrestrial stilling. This conclusion is also supported by the incoherency between the observed changes in u and LAI (regional, temporal and seasonal variations). As one of the drastic land use changes surrounding all *in situ* stations, urbanization plays a vital role in shaping the landscape on the Earth. The decrease of

near-surface wind speed is likely to be closely associated with the changing surface aerodynamic characteristics due to urbanization near the stations at regional scale (e.g. Zha *et al* 2017, Liu *et al* 2018). Future studies should be dedicated to exploring the connection of urbanization with the global wind stilling. A prerequisite is a high-resolution, temporal-consistent data product that can accurately capture the spatial and temporal patterns of urbanization over the globe.

Acknowledgments

ORCID iDs

Zhenzhong Zeng ⓘ https://orcid.org/0000-0001-6851-2756
Shilong Piao ⓘ https://orcid.org/0000-0001-8057-2292
Maofeng Liu ⓘ https://orcid.org/0000-0002-8340-0215

References

Cowie S M, Knippertz P and Marsham J H 2013 Are vegetation-related roughness changes the cause of the recent decrease in dust emission from the Sahel? *Geophys. Res. Lett.* **40** 1868–72

Daron J D and Stainforth D A 2013 On predicting climate under climate change *Environ. Res. Lett.* **8** 034021

England M H *et al* 2014 Recent intensification of wind-driven circulation in the pacific and the ongoing warming hiatus *Nat. Clim. Change* **4** 222–7

Fan *et al* 2014 Earlier vegetation green-up has reduced spring dust storms *Sci. Rep.* **4** 6749

Frost G V and Epstein H E 2014 Tall shrub and tree expansion in Siberian tundra ecotones since the 1960s *Glob. Change Biol.* **20** 1264–77

He J and Soden B J 2016 The impact of SST biases on projections of anthropogenic climate change: a greater role for atmosphere-only models? *Geophys. Res. Lett.* **43** 7745–50

Held I M and Soden B J 2006 Robust responses of the hydrological cycle to global warming *J. Clim.* **19** 5686–99

Horton D E, Johnson N C, Singh D, Swain D L, Rajaratnam B and Diffenbaugh N S 2015 Contribution of changes in atmospheric circulation patterns to extreme temperature trends *Nature* **522** 465–9

Hurrell J W *et al* 2013 The community Earth system model: a framework for collaborative research *Bull. Am. Meteorol. Soc.* **94** 1339–60

Kalma J D, McVicar T R and McCabe M F 2008 Estimating land surface evaporation: a review of methods using remotely sensed surface temperature data *Surv. Geophys.* **29** 421–69

Kelly M and Jørgensen H E 2017 Statistical characterization of roughness uncertainty and impact on wind resource estimation *Wind Energ. Sci.* **2** 189–209

Kim J and Paik K 2015 Recent recovery of surface wind speed after decadal decrease: a focus on South Korea *Clim. Dyn.* **45** 1699–712

Krinner G, Viovy N, de Noblet-Ducoudre N, Ogee J, Polcher J, Friedlingstein P, Ciais P, Sitch S and Prentice I C 2005 A dynamic global vegetation model for studies of the coupled atmosphere-biosphere system *Glob. Biogeochem. Cycles* **19** GB1015

Kosaka Y and Xie S P 2013 Recent global-warming hiatus tied to equatorial Pacific surface cooling *Nature* **501** 403–7

Liu J, Gao Z, Wang L, Li Y and Gao C Y 2018 The impact of urbanization on wind speed and surface aerodynamic characteristics in Beijing during 1991–2011 *Meteorol. Atmos. Phys.* **130** 311–24

Lorenz E N 1963 Deterministic nonperiodic flow *J. Atmos. Sci.* **20** 130–41

Marti O *et al* 2010 Key features of the IPSL ocean atmosphere model and its sensitivity to atmospheric resolution *Clim. Dyn.* **34** 1–26

McVicar T R and Roderick M L 2010 Atmospheric science: winds of change *Nat. Geosci.* **3** 747–8

McVicar T R, Van Niel T G, Li L T, Roderick M L, Rayner D P, Ricciardulli L and Donohue R J 2008 Wind speed climatology and trends for Australia, 1975–2006: capturing the stilling phenomenon and comparison with near-surface reanalysis output *Geophys. Res. Lett.* **35** L20403

McVicar T R *et al* 2012a Less bluster ahead? Ecohydrological implications of global trends of terrestrial near-surface wind speeds *Ecohydrology* **5** 381–8

McVicar T R *et al* 2012b Global review and synthesis of trends in observed terrestrial near-surface wind speeds: implications for evaporation *J. Hydrol.* **416–417** 182–205

Myneni R B *et al* 1997 Increased plant growth in the northern high latitudes from 1981 to 1991 *Nature* **386** 698–702

Nuijens L *et al* 2018 Implications of warm rain in shallow cumulus and congestus clouds for large-scale circulations *Shallow Clouds, Water Vapor, Circulation, and Climate Sensitivity* ed R Pincus *et al* (Berlin: Springer) pp 85–110

Peterson T C, Willett K M and Thorne P W 2011 Observed changes in surface atmospheric energy over land *Geophys. Res. Lett.* **38** L16707

Pryor S C, Barthelmie R J and Schoof J T 2006 Inter-annual variability of wind indices across Europe *Wind Energy* **9** 27–38

Pryor S C, Barthelmie R J, Young D T, Takle E S, Arritt R W, Flory D, Gutowski W J, Nunes A and Roads J 2009 Wind speed trends over the contiguous United States *J. Geophys. Res.* **114** D14105

Remote Sensing Systems 2015 Monthly mean wind speed data set on 1 degree grid made from Remote Sensing Systems Version 7 microwave radiometer data. Santa Rosa, CA, USA. www.remss.com/measurements/wind/wspd-1-deg-product/

Roderick M L, Rotstayn L D, Farquhar G D and Hobbins M T 2007 On the attribution of changing pan evaporation *Geophys. Res. Lett.* **34** L17403

Rousseeuw P J and Leroy A M 2005 *Robust Regression and Outlier Detection* (New York: Wiley)

Shinozaki K, Yoda K, Hozumi K and Kira T 1964 A quantitative analysis of plant form-the pipe model theory: I. Basic analyses *Jpn. J. Ecol.* **14** 97–105

Sparks P R, Schiff S D and Reinhold T A 1994 Wind damage to envelopes of houses and consequent insurance losses *J. Wind Eng. Ind. Aerodyn.* **53** 145–55

Su Z, Schmugge T, Kustas W P and Massman W J 2001 An evaluation of two models for estimation of the roughness height for heat transfer between the land surface and the atmosphere *J. Appl. Meteorol.* **40** 1933–51

Tape K E N *et al* 2006 The evidence for shrub expansion in Northern Alaska and the Pan-Arctic *Glob. Change Biol.* **12** 686–702

Taubert F, Fischer R, Groeneveld J, Lehmann S, Müller M S, Rödig E, Wiegand T and Huth A 2018 Global patterns of tropical forest fragmentation *Nature* **554** 519–21

Vautard R, Cattiaux J, Yiou P, Thepaut J and Ciais P 2010 Northern Hemisphere atmospheric stilling partly attributed to an increase in surface roughness *Nat. Geosci.* **3** 756–61

Vecchi G A and Soden B J 2007 Global warming and the weakening of the tropical circulation *J. Clim.* **20** 4316–40

Wentz F J, Ricciardulli L, Hilburn K and Mears C 2007 How much more rain will global warming bring? *Science* **317** 233–5

Wu J, Zha J, Zhao D and Yang Q 2018 Changes in terrestrial near-surface wind speed and their possible causes: an overview *Clim. Dyn.* **5** 2039–78

Xu L *et al* 2013 Temperature and vegetation seasonality diminishment over northern lands *Nat. Clim. Change* **3** 581–6

Young I R, Zieger S and Babanin A V 2011 Global trends in wind speed and wave height *Science* **332** 451–5

Zeng Z *et al* 2017 Climate mitigation from vegetation biophysical feedbacks during the past three decades *Nat. Clim. Change* **7** 432–6

Zeng Z *et al* 2018a Impact of Earth greening on the terrestrial water cycle *J. Clim.* **31** 2633–50

Zeng Z, Estes L, Ziegler A D, Chen A, Searchinger T, Hua F, Guan K, Jintrawet A and Wood E F 2018b Highland cropland expansion and forest loss in Southeast Asia in the twenty-first century *Nat. Geosci.* **11** 556–62

Zeng Z, Gower D B and Wood E F 2018c Accelerating forest loss in Southeast Asian Massif in the 21st century: a case study in Nan Province, Thailand *Glob. Change Biol.* **24** 4682–95

Zha J, Wu J and Zhao D 2017 Effects of land use and cover change on the near-surface wind speed over China in the last 30 years *Prog. Phys. Geogr.* **41** 46–67

Zheng C W, Pan J and Li C Y 2016 Global oceanic wind speed trends *Ocean Coast. Manage.* **129** 15–24

Zhu Z *et al* 2013 Global data sets of vegetation leaf area index (LAI) 3g and fraction of photosynthetically active radiation (FPAR) 3g derived from global inventory modeling and mapping studies (GIMMS) normalized difference vegetation index (NDVI3g) for the period 1981 to 2011 *Remote Sens.* **5** 927–48

Zhu Z *et al* 2016 Greening of the Earth and its drivers *Nat. Clim. Change* **6** 791–5